Simulation of the Particle Melting Degree in Air Plasma Spraying

K. Bobzin[1], M. Öte[1], M. A. Knoch[1], I. Alkhasli[1]*, U. Reisgen[2], O. Mokrov[2], O. Lisnyi[2]
[1] RWTH Aachen University, IOT - Surface Engineering Institute, Aachen, Germany

[2] RWTH Aachen University, ISF – Welding and Joining Institute, Aachen, Germany

E-mail: alkhasli@iot.rwth-aachen.de, *corresponding Author

Abstract. Plasma spraying is a coating process which is widely used for the application of thermal barrier coatings. High plasma jet temperatures allow the processing of ceramic material particles which characteristically exhibit low thermal conductivities. This, in turn, produces high temperature gradients inside the particles and vaporization on the particles' surface during their dwell time in the plasma jet. Thus, a single particle in the plasma-jet can exhibit 3 states of matter simultaneously: solid in the core, molten exterior and gaseous on the surface. The temperature distribution inside the particles is the foremost factor which influences the particles' behavior during their impact on the substrate surface. Experimental investigations can provide only the surface temperature of the particles, which is not a good indicator of the melting degree for ceramic particles due to the high temperature gradients. This study focuses on the determination of the temperature distributions inside the particles, during their flight in the plasma and the free jet, with the help of numerical simulations. For this purpose, a numerical model of the plasma spraying process that describes the plasma and the free jet loaded with sprayed particles is presented. The model includes three sub-models; a plasma torch sub-model, a particle-laden free jet sub-model and a powder particles sub-model. The first sub-model calculates the temperature and velocity fields of the plasma inside the plasma torch, the second sub-model the kinetics of temperature and velocity fields of the turbulent free jet generated by the plasma torch. This information is used in the third sub-model to calculate the kinetics of temperature distribution within the particles, their melting degree and mass losses due to evaporation. The third sub-model also calculates heat and mechanical impulse loses due to the particle-plasma interaction, which in turn is coupled with the free jet sub-model.

1. Introduction

The air plasma spraying process (APS) has been the subject of numerous numerical models which attempt to consider the whole complexity of the relevant physical phenomena. The simulation of a single cathode plasma spraying systems involves transient models of the arc root fluctuations at the anode [1, 2] and the effect of plasma fluctuations on the particle temperature and velocity [3, 4]. In a three-cathode APS system, the arc root fluctuations are vastly diminished by a special placement of neutrode rings and the anode. This allows steady-state simulations of such systems [5, 6]. Steady-state simulations of a three-cathode APS system often consider the dispersion of the particles at the injector exit, the influence of the powder carrier gas flow on the plasma flow as well as the particle distribution in the plasma jet [7]. Relevant are the distributions of the size, the velocity and the temperature of the

particles in the plasma jet [6, 8]. The most common approach for the determination of the particle temperatures is the lumped capacitance method which assumes a homogenous temperature within the particle [9, 10, 11]. For materials with a high thermal conductance such as metals, especially for particles smaller than 100 µm in diameter, this assumption seems plausible and delivers results close to reality. However, ceramic materials, which are commonly used in APS applications, usually have a significantly lower thermal conductance than metals [12]. This causes substantial temperature gradients between the particle surface and its core. A ceramic particle which is molten on its surface but still has a solid core is a commonplace phenomenon in APS which was taken into account in various simulations by considering heat transfer within the particles [13, 14, 15, 16, 17, 18, 19]. An inhomogeneous melting of ceramic particles has a significant effect on the bonding behaviour and the porosity of the final coating and is therefore considered in this study.

State of the art particle diagnostics in thermal spraying does not provide information regarding the temperature gradients in the particle [20]. Temperature measurements, which are based on the two-colour pyrometry, rely on the emission values on the particle surface [21]. Accordingly, they deliver only the surface temperature of the particle. It's a known case, that an increase of the electrical current in the plasma generator might deteriorate the deposition efficiency of the spraying process. The reason is that increasing the current increases not only the plasma temperature, but also the plasma velocity. This, in turn contributes to the increase in particle velocities and therefore, to the decrease of the particle dwell times in the plasma jet [6]. In such cases, experimental measurement of the particle temperature indicates temperatures above the melting point of the spray material, nonetheless the solid core springs back off the substrate surface. The aim of this study is to develop a numerical model for the heat conduction and the phase change phenomena in order to determine the temperature distribution and the location of the melt front within the particles during their flight in the plasma jet. This will contribute to the understanding of the bonding behaviour of ceramic particles in APS which in turn would enable the prediction of deposition efficiency and coating porosity. In the next section, the modelling of the plasma and the free jet will be described, followed by the description of the modelling of sprayed particle. Input parameters that are used in the simulations are presented in the "Model Parameters and Boundary Conditions" section. The results of the simulations and their analysis are presented in the "Results and Discussions" section which is followed by the Conclusion.

2. Modeling of Plasma and Free Jet

In this section, the numerical model that was used to describe the physical phenomenon in the plasma torch and the free jet as well as the boundary conditions will be described. The underlying principle of a plasma torch is based on the ionisation of a working gas between the electrodes by applying an electrical potential difference between the electrodes. This causes the gas to ionise and form an electrically conductive path between the electrodes. Thus, the conversion of the electrical energy into heat energy is achieved in the plasma generator. After being converted into the plasma state, the process gas leaves the nozzle of the plasma generator at high temperatures (T_P > 12,000 K) and velocities (v_P > 1,000 m/s) [7].

2.1 Boundary conditions and model parameters

In this work, the three-cathode plasma torch TriplexPro™-210 from Oerlikon Metco is analysed. It has 24 radially placed inlets which pass the operating gas into the convergent part of the plasma torch while the inclination of the inlets causes the gas to swirl. The anode ring which is located next to the torch outlet is separated from the cathodes with a long tubular section of neutrode rings. The geometry of the interior of the plasma generator is depicted in the Figure 1. The plasma torch allows the injection of the particles into the plasma flame from three radially placed injectors downstream to the outlet.

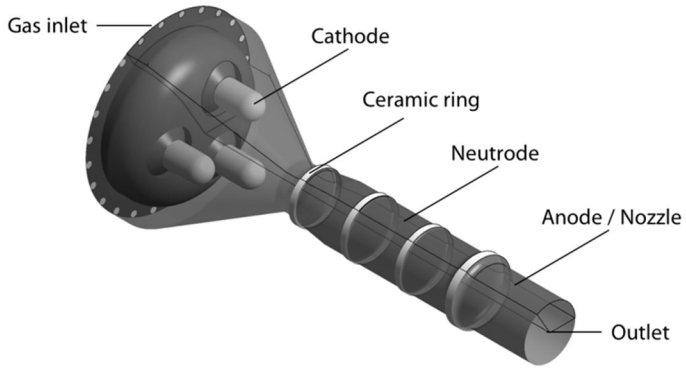

Figure 1. Interior geometry of the plasma generator TriplexPro™-210 torch from Oerlikon Metco GmbH (Kelsterbach, Germany)

The plasma simulation in the plasma torch is already an established model [5–7] and is coupled with the free jet simulation [8]. The boundary conditions of the free jet are the plasma flow profiles at the plasma torch outlet. The flow profiles are exported from the plasma torch simulation and imported into the free jet simulation as a boundary condition. The flow properties that are imported to the free jet simulation at the plasma torch nozzle are the velocity profile, total temperature, turbulent kinetic energy and turbulent eddy dissipation.

Generally speaking, there are several approaches to plasma modelling which include single particle, kinetic, fluid, hybrid kinetic/fluid, gyrokinetic and system of many particles. Kinetic and fluid models are the most widely used ones in the literature [2, 3, 5, 6]. While the kinetic description of the plasma delivers more accurate results, due to its complexity and the computational overhead associated with it, the fluid model of the plasma is considered in this work. The fluid model describes the plasma based on the macroscopic parameters, which are determined by coupling the mass, momentum and energy conservation equations with the Maxwell equations. A commercial general-purpose CFX package Ansys CFX® (Release V15) was employed for the calculation of the plasma behaviour in this study. The following system of equations has to be solved numerically in order to describe the plasma flow:

$$\frac{\partial \rho}{\partial t} + \nabla(\rho \vec{u}) = 0, \tag{1}$$

$$\rho\left(\frac{\partial \vec{u}}{\partial t} + \vec{u}\nabla\vec{u}\right) = \rho\vec{g} + \nabla\vec{\tau} - \nabla p + \overrightarrow{f_L} + S_V, \tag{2}$$

$$\frac{\partial \rho h}{\partial t} + \nabla(\rho h \vec{u}) = \nabla\left(\frac{\lambda}{C_p}\nabla h\right) + S_{Joule} + S_{Net} + S_H, \tag{3}$$

$$S_{Net} = S_{Rad} + S_{Abs} \tag{4}$$

The first three equations describe the thermodynamic fluid flow of the plasma and are equations of conservation of mass (Eq. 1), momentum (Eq. 2) and energy (Eq. 3) and are coupled with the Maxwell equations of electromagnetism. The coupling between the electromagnetic forces and the fluid flow dynamics is defined by the Lorentz force, the Joule heating which describes the electric heating of the process gas in the plasma torch as well as the radiation model. Radiation is modelled according to the temperature and pressure dependent net emission coefficient model. The values for the coefficient is taken from the literature [22, 23]. The momentum loss of the free jet due to the particle is taken into account with the term S_V. The term S_H in the Eq.(3) corresponds to the heat exchange between the plasma jet and the particle. S_V and S_H will be addressed in chapter 3.4 in more detail.

In order to predict the magneto hydrodynamic behaviour of the plasma column in the plasma generator, the temperature and pressure dependent properties of the plasma gas are included in the calculations. Properties of the most common operating gases in thermal spray are available in the literature [24, 25]. In order to model the turbulent mixing and the heat dissipation in the turbulent plasma flow, the two-equation turbulence SST model is used.

Because of the high plasma temperatures, the losses due to the radiation are significant in the total heat balance of the plasma flow. The net emission coefficient model was employed for the calculation of the radiation losses according to [5, 6]. The radiation energy balance is defined as the difference between the emitted and the absorbed radiation which is in turn a temperature and pressure dependent term of the energy conservation equation. This model calculates the radiation losses according to the temperature and pressure distribution in the simulation domain. The radiative warming of colder regions is neglected due to the low radiative absorption of the surrounding gases. The input parameters for the plasma jet model are given in the Table 1:

Table 1. Input parameters for the particle-laden plasma-jet model

Property	Unit	Value
Plasma gas		Argon
Arc current	A	500
Gas flow rate	SLPM	50
Nozzle diameter	mm	9
Carrier gas flow rate	g/s	0.15
Particle injection rate	g/s	0.4
Particle mean diameter	µm	38
Particle diameter standard deviation	µm	11

3. Modelling of Sprayed Particles

The mathematical model of the particle behaviour in the plasma jet is described by the equations of transient heat transfer, balance of mass, movement and interaction conditions with the free jet. The main assumptions that are used for the particle description are listed below:

- spherical particle geometry
- particle temperature distribution has a spherical symmetry
- local plasma temperature and velocity along the boundary layer of particles are constants and defined by the current particle mass center position in the free jet
- particle size can vary due to evaporation
- particle evaporation has no influence on heat exchange between the particle and flow jet
- temperature and velocity fields of the free jet are given and calculated according to a-priori simulations as shown in [5, 6].

Besides the boundary conditions, each particle is defined by a set of initial conditions. The most important ones are:

- initial radius R_0
- initial temperature T_0
- coordinates of the injection (point A in Figure 2)
- initial particle velocity at point A

Additional parameters are the volume flow rate of the carrier gas, diameter of the particle injector, particle mass feed rate, maximal distance of the particle movement along the free jet direction and the temperature dependent material properties of the particle (Table 3). The coefficients and constants used for the free jet and the particle heating simulations are listed in Table 2.

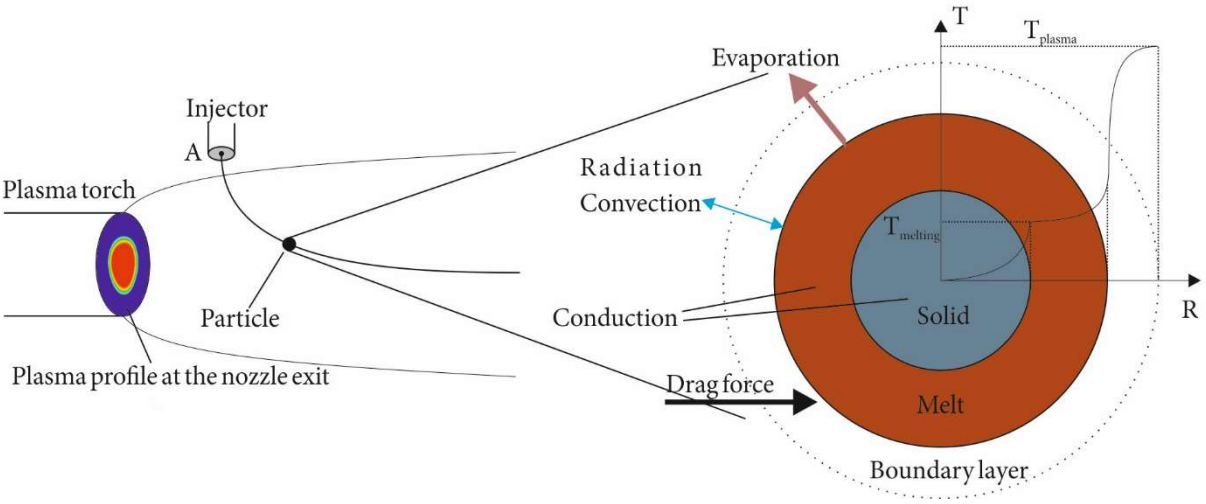

Figure 2. Schematic description of the discrete particle traveling in free jet and the particle heating model

Table 2. Coefficients and constants used in the simulations

Property	Symbol, unit	Value
Stefan-Boltzmann constant	σ, W cm^{-2} K^{-4}	5.67 10^{-4}
coefficient of radiation emission	ε_σ	0.6
gravitational acceleration	*g*, cm s^{-2}	980.0
ambient temperature	T_0, K	293.15
ambient pressure	*p,* bar	1.013

3.1 Particle heating

Particle heating in a free jet is described by the heat equation written in spherical coordinates, with its origin located at the particle center [26]. The heat equation is written one dimensional form due to the spherical symmetry assumption of the particles.

$$\frac{\partial H}{\partial t} = \frac{1}{r^2}\frac{\partial}{\partial r}\left(r^2 \lambda \frac{\partial T}{\partial r}\right), \qquad (5)$$

$$0 < r < R, \quad t_A < t < t_L$$

$$H = \rho \int_{T_0}^{T} c\, dT + \rho \chi_m \qquad (6)$$

Here, *H(T)* – is enthalpy, *T* – temperature, *R* – the instantaneous radius of the particle, *t* - the particle heating time, t_A –time at the point A (Figure 2), t_L – time at the axial distance *L* and λ - thermal conductivity. Enthalpy is described by the Eq. (6), where *c* – is heat capacity, ρ – density, χ_m - latent melting heat. Boundary conditions are defined as:

$$\left.\frac{\partial T}{\partial r}\right|_{r=0} = 0 \tag{7}$$

$$\lambda_p \left.\frac{\partial T}{\partial r}\right|_{r=R} = q - \chi_v g_v \tag{8}$$

$$q = \alpha(T_g - T(R)) + \xi\sigma_0(T_g^4 - T(R)^4) \tag{9}$$

where q is the heat flow from the gas into the particle, with the coefficient of convective heat exchange between the particle and free jet α and radiative heat exchange via the emissivity factor ξ. T_g is the gas temperature at the particle location and $T(R)$ is the particle surface temperature. χ_v is the heat of vaporization, $g_v(T)$ - specific surface mass flow rate of vaporization and σ_0 the Stefan-Boltzmann constant.

3.2 Particle size

Since the evaporation at the particle surface was taken into account, the particle radius may change. At each time increment the instantaneous particle radius defined by the mass balance equation:

$$\frac{dm}{dt} = g_v S \tag{10}$$

with the particle mass $m = 4/3\pi R^3\rho$ and the particle surface areas $S = 4\pi R^2$. The impact of the surface evaporation on the overall particle mass will be a subject of further studies.

3.3 Particle velocity and trajectory

The particle velocity and trajectory can be obtained by the equating Newton's second law to the aerodynamical drag force acting on the particle surface during its flight in the free jet. For this purpose, the velocity of discretely defined particles is determined as the time derivative of the particles' centre coordinates. The equations are written as follows:

$$\frac{d(m\vec{v})}{dt} = \vec{\mathbf{F}} \tag{11}$$

$$\vec{\mathbf{F}} = C_d S_m \frac{\rho_g (\vec{u} - \vec{v})|\vec{u} - \vec{v}|}{2} + m\vec{g} \tag{12}$$

where $\vec{v}$ – is the particle velocity; $\vec{u}$ – is the local free jet velocity which takes into account the interaction with sprayed particle; $\vec{\mathbf{F}}$ – is the aerodynamical drag force vector; C_d – is the drag coefficient of a spherical particle; $S_m = \pi R^2$ – is the cross-sectional area of a spherical particle; ρ_g - is the density of surrounding gas; $\vec{g}$ - is the gravitational acceleration.

Different approaches exist for the description of the coefficients of convective heat exchange and aerodynamical drag for a spherical particle. A comparison regarding the influence of the different descriptions of the coefficients is presented in [27]. In this work, the description of coefficients according to [26] is employed as depicted in equations (13-17).

$$\alpha = Nu \frac{\lambda_g}{2R} \tag{13}$$

$$C_d = \begin{cases} 24\,\mathrm{Re}^{-1}, & \mathrm{Re} \le 0.2 \\ 24\,\mathrm{Re}^{-1} + 3.6\,\mathrm{Re}^{-0.317}, & 0.2 < \mathrm{Re} \le 4.0 \\ 24\,\mathrm{Re}^{-1} + 4\,\mathrm{Re}^{-0.333}, & 4.0 < \mathrm{Re} \end{cases} \quad (14)$$

$$Nu = 2\frac{\lambda_g}{\lambda} + 0.5\,\mathrm{Re}^{0.5}\,\mathrm{Pr}^{0.4}\left(\frac{\rho_g\big|_{r>>R}\,\eta_g\big|_{r>>R}}{\rho_g\big|_{r=R}\,\eta_g\big|_{r=R}}\right)^{0.2} \quad (15)$$

$$\mathrm{Re} = 2R\,\rho_g|u - v|/\eta_g \quad (16)$$

$$\mathrm{Pr} = C_g\eta_g/\lambda_g \quad (17)$$

where Nu - is the Nusselt number; Re - the Reynolds number; Pr- the Prandtl number; η - dynamic viscosity of the free jet; λ_g, ρ_g, η_g, C_g - are the free jet properties at the point of the particle location, calculated at the particle surface temperature.

3.4 Influence of the sprayed particles on the free jet

The particles injected into the free jet are accelerated and heated by the gas. At the same time the free jet is slowed and cooled down due to the influence of the injected particles [28]. In order to take into account this effect the "two-way coupling" method is implemented. This is achieved by coupling the equations of momentum (equation (2)) and energy (equation (3)) of the fluid flow with the momentum and energy equations of the particle with the help of the terms S_V and S_H. These terms incorporate the momentum and energy loss due the acceleration and heating up the particles into the free jet flow and are defined as:

$$S_v = \frac{1}{\delta V}\sum_{k=1}^{b}\vec{\mathbf{F}}_k S_k \quad (18)$$

$$S_H = \frac{1}{\delta V}\sum_{k=1}^{b} q_k S_k \quad (19)$$

$$n_t = \frac{3}{4\pi R_0^3}\frac{G_M}{\rho} \quad (20)$$

where S_V, S_H are the local values of the free jet heat and mechanical impulse loss due to the interaction of the free jet with the particles; b – is the instantaneous number of particles that are locally present in a free jet volume δV; n_t – is the integer part of the amount of the particles homogenously distributed on the diameter of the injector nozzle and G_M is the particle feed rate. Initial condition of the particle loading of the plasma flow is defined by $S_V = 0$, $S_H = 0$, $G_M = 0$.

3.5 Material properties used in the particle heating model

The model described by equations (5 - 20) enables the calculation of the particle velocity, particle trajectory and kinetics of radial temperature distribution in the particle, the ratio of its melting and mass losses due to evaporation. These particle parameters can be calculated in dependence on the material composition, initial temperature and the particle diameter, particle feed rate and further conditions of particle injection into the plasma jet. Besides, this model can be used to observe the behaviour of multiple particles simultaneously. The material properties of the powder particle used in the simulation were chosen according to [28] and are shown in Table 3:

Table 3. Material properties of the feedstock material [28]

Property	Symbol, unit	Value
Material		Al_2O_3
Melting temperature	T_M, K	2,345
Boiling temperature	T_B, K	3,250
Latent heat of melting and solidification	χ_m, J g^{-1}	1,150
Latent heat of vaporization	χ_v, J g^{-1}-	19,380
Material density	ρ, g cm^{-3}	3,690
Heat capacity	c , J g^{-1} K^{-1}	1.2
Thermal conductivity	λ, W cm^{-1} K^{-1}	0.3

4. Results and Discussion

A plasma generator simulation was conducted using the parameters indicated in the section 2.1. The velocity and temperature fields at the plasma generator nozzle exit were transferred to the free jet simulation as boundary conditions. Flow conditions at the nozzle exit served as an inlet condition for the free jet computational domain. Figure 3 illustrates the trajectories of the particles injected into the free jet with an indication of the particle temperatures during their flight. Particle temperatures shown in the figure were obtained using the lumped capacitance method.

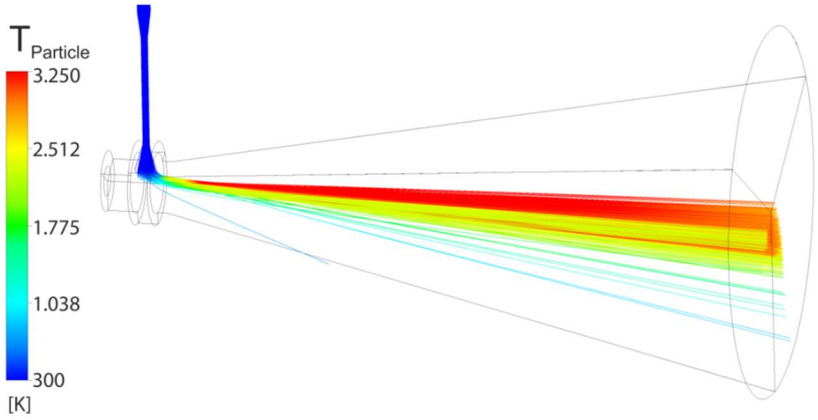

Figure 3. Temperature distribution and trajectories of the particles in the plasma and the free jet

Temperature gradients within particles were calculated exemplarily for the particles of $D = 22$ µm and $D = 60$ µm diameter and their temperature variations were compared. Gas temperatures and velocities as well as the particle velocities in the free jet at instantaneous particle coordinates were used as boundary conditions in order to calculate the temperature variation inside the particles. Temperature distributions between the particle cores and their surfaces are shown in Figure 4, where

r/R represents the particle radial coordinate normalised with respect to the initial particle radius. Since the temperature distribution of a particle in flight changes continuously, the temperature distributions are depicted at different stand-off distances y, which is the axial distance between the plasma generator nozzle and the instantaneous coordinate of the particle during its flight. For both particles, it can be seen that the particle surfaces warm up rapidly and reach high temperatures very near the plasma generator nozzle while the particle core remains cold. The temperature difference between the particle core and its surface levels out as it travels further along its flight trajectory. For the smaller particle, the particle core temperature reaches the melting temperature at $L = 17$ cm stand-off distance, whereas the core of the larger particle does not melt during the whole time of its flight.

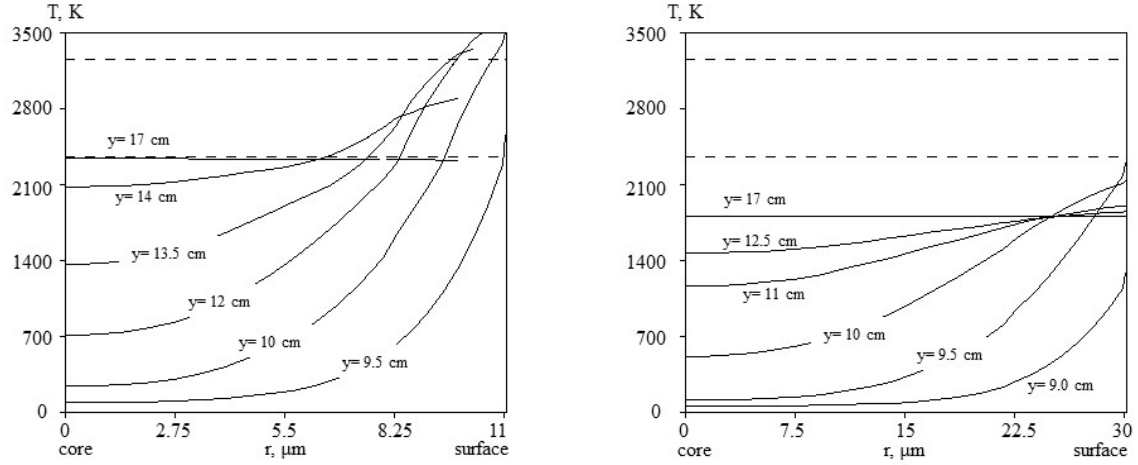

Figure 4. Variation of particle temperatures for particles of $\boldsymbol{D = 22}$ **μm** and $\boldsymbol{D = 60}$ **μm** diameter where y corresponds to the axial distance between the plasma generator nozzle and the particle in-flight position

Another way to compare small and large particles is to plot the temperature at the particle surface and its core against the distance travelled by the particle in flight. Figure 5 illustrates rapid increase of the surface temperature near the nozzle which can be explained by high plasma temperatures in the vicinity of the plasma generator nozzle. As the particles travel to the cooler regions of the free jet the surface temperatures sink and the core temperatures increase due to the thermal conductance within the particles. The temperature inside the considered particles levels out at a distance of approximately $L = 15$ cm from the nozzle, independent of the particle size. Surface and the core temperatures meet slightly above the melting point of Al_2O_3 for the smaller particle, whereas temperature is levelled out at a temperature below the melting point for the larger one. The proof of concept model developed in this work does not include the latent heat of melting. The model developed in this work has shown the significance of the heat transfer within the particle because the temperature calculated according to the lumped capacitance model holds true only starting from the $L = 15$ cm from the nozzle, which is longer than the usual spraying distance. At shorter distances the actual temperature within the particle can vary by several hundreds of degrees from the temperature determined by the lumped capacitance method.

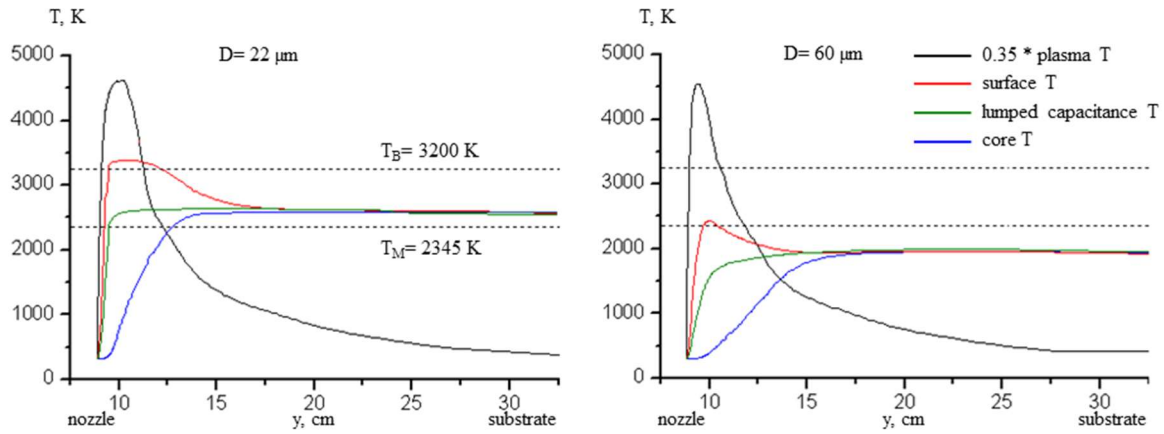

Figure 5. Temperature variation of the plasma, surface and the core of the particles as well as the particle temperature according to the lumped capacitance method during their free flight. The plasma temperature has been scaled down for better visibility

5. Summary and Outlook

In this work, the first model for the determination the temperature gradients within particles in a free jet was developed and simulated using a small and a large particle along their flight trajectory. To achieve this, three simulation models were coupled with each other. The first coupling took place between the simulation of the plasma generator and the free jet by exporting the flow profiles at the plasma generator nozzle as an inlet boundary condition for the free jet simulation. For the second coupling, gas temperatures and velocities at the immediate vicinity of the particle as well as particle velocity were used as boundary conditions for the transient heat transfer simulation within the particle along its flight trajectory. For the examined process parameters, the temperature gradients inside the small and the large particles diminish at around $\boldsymbol{L = 15\ cm}$ from the nozzle and the temperature of the particles become uniform. The smaller particle is completely molten at the end of the flight trajectory, whereas the core of the larger one remains solid during the whole flight. The influence of latent heat was neglected in the presented simulation. Since it is expected to be of relevance, a more sophisticated model accounting for the latent heat is in development.

6. Acknowledgements

All presented investigations were conducted in the context of the Collaborative Research Centre SFB1120 "Precision Melt Engineering" at RWTH Aachen University and funded by the German Research Foundation (DFG). For the sponsorship and the support we wish to express our sincere gratitude.

References

[1] Trelles JP, Chazelas C, Vardelle A, Heberlein JV, 2009 Arc plasma torch modeling. *Journal of Thermal Spray Technology:*728–52, 18.
[2] Fauchais P, 2004 Understanding plasma spraying. *J. Phys. D: Appl. Phys.:*R86-R108. doi:10.1088/0022-3727/37/9/R02, 37.
[3] Baudry C, Vardelle A, Mariaux G, Delalondre C, Meillot E, Three-dimensional and time-dependent model of the dynamic behavior of the arc in a plasma spray torch. In: ITSC 2004: International Thermal Spray Conference 2004: Advances in Technology and Application.
[4] Chazelas C, Moreau E, Mariaux G, Vardelle A, 2006 Numerical modeling of arc behavior in a DC plasma torch. *High Temperature Material Processes: An International Quarterly of High-Technology Plasma Processes*, 10.
[5] Bobzin K, Öte M, 2015, A Numerical Investigation: Air Plasma Spraying by means of a Three-Cathode Spraying Torch. In: International Thermal Spray Conference and Exposition (ITSC).
[6] Bobzin K, Öte M, 2016 Modeling Multi-Arc Spraying Systems. *J Therm Spray Tech:*920–32. doi:10.1007/s11666-016-0407-7, 25.
[7] Bobzin K, Kopp N, Warda T, Schäfer M, Öte M A Numerical Investigation: Influence of the Operating Gas On the Flow Characteristics of a Three-Cathode Air Plasma Spraying System. In: International Thermal Spray Conference and Exposition (ITSC).
[8] Bobzin K, Öte M, Schein J, Zimmermann S, Möhwald K, Lummer C, 2016 Modelling the Plasma Jet in Multi-Arc Plasma Spraying. *Journal of Thermal Spray Technology:*1111–26, 25.
[9] Vardelle M, Vardelle A, Leger A. C, Fauchais P, Gobin D, 1995 Influence of particle parameters at impact on splat formation and solidification in plasma spraying processes, *Journal of Thermal Spray Technology:* 50-8, 4. doi:10.1007/BF02648528
[10] Pasandideh-Fard M, Pershin V, Chandra S, Mostaghimi J, 2002 Splat shapes in a thermal spray coating process: Simulations and experiments, *Journal of Thermal Spray Technology:* 206-17, 11. doi:10.1007/BF02648528
[11] Khelfi D, El-Hadj AA, Aït-Messaoudène N, 2008 Modeling of a 3D plasma thermal spraying and the effect of the particle injection angle, *Revue des Energies Renouvelables CISM'08:* 205-16.
[12] Bobzin K, 2013 Oberflächentechnik für den Maschienenbau. Germany: Weinheim Wiley-VCH Verlag.
[13] Ahmed I, Bergman T. L, 2000 Three-dimensional simulation of thermal plasma spraying of partially molten ceramic agglomerates, 215-24, 9. doi:10.1361/105996300770349953
[14] McKelliget JW, Trapaga G, Gutierrez-Miravete E, Cybulski M, 1998 An integrated mathematical model of the plasma spraying process, *Thermal Spray: Meeting the Challenges of the 21st Century:* 335-40, 1.
[15] Chen X, Chyou YP, Lee YC, Pfender E, 1985 Heat Transfer to a Particle under Plasma Conditions with Vapor Contamination from the Particle, *Plasma Chemistry and Plasma Processing*: 119-41, 5.
[16] Wan YP, Prasad V, Wang G-X, Sampath S, Fincke JR, 1999 Model and Powder Particle Heating, Melting, Resolidification, and Evaporation in Plasma Spraying Processes, *Journal of Heat Transfer*: 691-9, 121.
[17] Li M, Shi D, Christofides PD, 2005 Modeling and control of HVOF thermal spray processing of WC–Co coatings, *Powder Technology:* 177-94, 156.
[18] Saha K, Chaudhuri S, Cetegen BM, 2011 Modeling of Ceramic Particle Heating and Melting in a Microwave Plasma, *Journal of Heat Transfer:* 133. doi: 10.1115/1.4002448
[19] Dyshlovenko S, Pawlowski L, Pateyron B, Smurov I, Harding JH, 2005 Modelling of plasma particle interactions and coating growth for plasma spraying of hydroxyapatite, *Surface and Coatings Technology:* 3757-69, 200.
[20] Zhang W, 2008 Integration of Process Diagnostics and Three Dimensional Simulations in Thermal Spraying; Dissertation.
[21] Fauchais P, Vardelle M, 2010 Sensors in Spray Processes. *Journal of Thermal Spray Technology:*668–94.
[22] Bauder U, 1968 Radiation from high - pressure plasmas. *Journal of Applied Physics:*148–52, 39.
[23] Menart J, Malik S 2002 Net emission coefficients for argon-iron thermal plasmas. *J. Phys. D: Appl. Phys.:*867–74, 35. doi:10.1088/0022-3727/35/9/306.
[24] Murphy AB, Arundelli CJ, 1994 Transport coefficients of argon, nitrogen, oxygen, argon-nitrogen, and argon-oxygen plasmas. *Plasma Chemistry and Plasma Processing:* 451–90, 14.
[25] Murphy AB, Tam E, 2014 Thermodynamic properties and transport coefficients of arc lamp plasmas: argon, krypton and xenon. *Journal of Physics D: Applied Physics*: 47.29

[26] Borisov Y, Bushma A, Krivtsun I, 2006 Modeling of motion and heating of powder particles in laser, plasma, and hybrid spraying. *Journal of Thermal Spray Technology:*553–8, 15.
[27] Öte M, 2016 Understanding Multi-Arc Plasma Spraying. 1. Auflage. Herzogenrath: Shaker, Dissertation ISBN 978-3-8440-4598-7
[28] Lamoreaux RH, Hildenbrand DL, Brewer L, 1987 High - Temperature Vaporization Behavior of Oxides II. Oxides of Be, Mg, Ca, Sr, Ba, B, Al, Ga, In, Tl, Si, Ge, Sn, Pb, Zn, Cd, and Hg. *Journal of physical and chemical reference data:*419–43, 16.